Thin–Walled Structures 231 (2026) 115625

Contents lists available at ScienceDirect

Thin-Walled Structures

journal homepage: www.elsevier.com/locate/tws

Full length article

Elastic instabilities in soft layered composites with alternating interlayer spacing

Viacheslav Slesarenko

Cluster of Excellence livMatS @ FIT – Freiburg Center for Interactive Materials and Bioinspired Technologies, University of Freiburg, Freiburg, 79110, Germany
Department of Microsystems Engineering, University of Freiburg, Freiburg, 79110, Germany

ARTICLE INFO

Keywords:
Layered composites
Elastic instabilities
Bloch–Floquet analysis

ABSTRACT

Elastic instabilities, once regarded purely as a failure mode, are now routinely harnessed to program the response of soft architected materials. Here we show that the onset of buckling in a layered composite can be tuned without changing how much stiff material it contains, simply by rearranging the layers. We consider laminates in which stiff layers, embedded in a soft matrix, are separated by two alternating gaps. We analyse their stability with an analytical model, a complementary sandwich-beam approximation for closely spaced layers, and Bloch–Floquet finite element simulations. At a fixed volume fraction, the evenly spaced (periodic) arrangement is the most stable, whereas the critical strain is lowest when the smallest gap becomes comparable to the layer thickness. By comparing the two extreme arrangements, we find that the periodic composite switches from short-wavelength wrinkling to long-wavelength macroscopic buckling at a lower volume fraction than the least stable arrangement, leaving a window in which the two arrangements fail in qualitatively different ways. Deviating from perfect periodicity thus offers some degree of tunability, but in practical applications one must not uncritically rely on predictions from periodic composites if periodicity during manufacturing cannot be guaranteed.

1. Introduction

The loss of stability has been historically treated on par with failure, which must be avoided in the engineering systems at any cost. Indeed, the buckling is associated with loss of the major fraction of the load-bearing capacity of the structures [1], and in laminated composites it is often closely linked to delamination, which both originates from and promotes local buckling [2]. At the same time, it has recently become apparent that the significant changes in the shape and mechanical properties that accompany the loss of the stability can be purposefully harnessed in the design of new materials [3–7]. In contrast with the failure/fracture, the elastic buckling is a reversible process, and the removal of the external load usually restores the initial shape of the material. Simultaneously, the loss of stability enables effects such as bistability, allowing the coexistence of multiple stable states [8]. Therefore it is not surprising that the instability-inspired motifs can be traced in the design of modern mechanical metamaterials [9–12] and architected structures [13–16]. Despite the variety of design ideas enabling advanced behaviour in metamaterials [17–21], the simple elastic buckling continues to be one of the most exploited phenomenon. The local buckling was not only useful to create the materials with variable stiffness [22–24], but was also successfully employed to harvest elastic energy, control propagation of the elastic waves, and create multistable systems [25–29].

While materials and structures of various designs can undergo buckling, laminated and fibre composites remain, probably, the most studied ones. Starting from the early studies of fibre and layer microbuckling [30,31], each subsequent work increased the understanding of the elastic instabilities phenomena in layered and fibre composites. The onsets of macroscopic instabilities, characterised by wavelengths significantly larger than the microstructure characteristic size, in hyperelastic media, were studied using loss of ellipticity analysis combined with a phenomenological material model for transversely isotropic fibre composites under compression [32–34]. Micromechanics-based homogenisation has also proved to be an effective tool for predicting the onset of macroscopic instabilities [35]. More involved Bloch–Floquet technique was successfully implemented to search for the microscopic (as well as macroscopic) instabilities in the fibrous and layered media [31,36–38], and has since been applied to a broad range of soft periodic composites [39–42]. The competition between local wrinkling and global long-wave buckling in multi-layered composites has by now been examined both theoretically and experimentally, and the conditions selecting one mode or the other have been mapped

E-mail address: viacheslav.slesarenko@livmats.uni-freiburg.de.
URL: https://slesarenko-lab.com.

https://doi.org/10.1016/j.tws.2026.115625
Received 30 June 2026; Received in revised form 17 August 2026; Accepted 2 September 2026
Available online 9 September 2026
0263-8231/© 2026 The Author. Published by Elsevier Ltd. This is an open access article under the CC BY license (http://creativecommons.org/licenses/by/4.0/).

over a broad parameter space [43–46]. In general, this framework has been extended to rate-dependent constituents, revealing the role of viscoelasticity in microstructural buckling of soft particulate composites [47] and of visco-hyperelastic laminates [48,49]. Moreover, due to the intrinsic connection between instabilities and elastic waves, the Bloch–Floquet analysis simultaneously enables an efficient way to study the propagation of elastic waves prior to [27], in the vicinity of [50], and in the post-buckling regime of instabilities [51].

As shown for instance in [40,48,51], for the relatively simple composite geometries and under small or moderate deformation the difference between the stability of composites with elastic (Hookean) and hyperelastic (neo-Hookean) is not significant. For the periodic layered composites with linear elastic constituents, the rigorous study by Parnes and Chiskis [52], provides accurate estimates of the onsets of macroscopic and microscopic instabilities using direct stress and strain calculations for stiff and soft constituents. At the same time, even under linear elastic assumption, the previous studies were mostly focused on the analysis of the stability for fibre and layer composites with either strictly periodic structure [31,52,53], or randomly distributed stiff layers/fibres [54]. A separate line of work concerns not the arrangement of the layers but what is located between them. Introducing a third phase of finite thickness between the stiff layer and the matrix strongly affects the onset of buckling, and such three-phase laminates exhibit a rich variety of coexisting instability modes whose selection is governed by the stiffness and the thickness of the intermediate layer [55–59]. Here, we show that by keeping the volume fraction of the stiff phase constant and deviating from the ideally periodic geometry, the stability of the layered composites can be tuned. The considered geometry can be seen as a minimal viable case of composites and instability-driven metamaterials in which the onset of buckling is altered purely by the arrangement of the layers, while the constituents, their amount and the thickness of the layers all remain unchanged. In particular, we consider layered composites with alternating distances between the layers. This arrangement lies between two classical arrangements – strictly periodic and fully random. We reveal both analytically and numerically that the composite with ideal periodicity is the most stable, while the lowest critical strain corresponds to the geometry in which the distance between the closest neighbouring layers is equal to the thickness of the stiff layers. By modifying the periodicity we show how the stability of the layered composite might deteriorate even while the volume fraction remains constant. The relative simplicity of this geometry allows us to extend the classical analysis [52] to the case of two unequal gaps and to obtain a closed-form estimate of the critical strain, from which an explicit expression for the least stable arrangement follows. We further demonstrate that the transition between microscopic wrinkling and macroscopic long-wave buckling occurs at different volume fractions for the two limiting arrangements, leaving a finite window in which composites with the same composition lose stability in qualitatively different ways.

2. Geometry and materials

The geometry of conventional periodic laminate composites in two dimensions can be defined through only two parameters, for instance a period and volume fraction of the stiff phase. In the case of the layered composites, that are considered in this manuscript, the introduction of the additional parameter describing the ratio of the distances between left and right neighbours of the selected layer is needed. We refer to such laminates, in which the stiff layers retain a common period but the spacing between successive layers alternates between two values, as layered composites with alternating interlayer spacing (Fig. 1a). To describe the geometry of the considered composites consisting of the layers/fibres with thickness c_f, separated by gaps of thicknesses c_m^1 and c_m^2, we introduce two parameters: volume fraction of layers $v_f = 2c_f/(2c_f+c_m^1+c_m^2)$ and ratio between gap thicknesses $f = c_m^1/c_m^2 \leq 1$ (without loss of generality, $c_m^1 \leq c_m^2$ and $f \leq 1$).

For some derivations it is favourable to introduce another parameter $q = c_m^1/c_f$ to describe the relation between the minimal gap and the thickness of the layers. The three geometric factors v_f, f and q are mutually connected as follow

$$f = \frac{qv_f}{2 - qv_f - 2v_f} \tag{2.1}$$

Throughout the manuscript the constituents of the layered composites are considered to be linear elastic (if not mentioned opposite), with $E_m = 1$ MPa and $\nu_m = 0.49$ the Young's modulus and Poisson's ratio for the soft matrix material, respectively, and E_f and ν_f being the Young's modulus and the Poisson's ratio of stiff material, correspondingly. For following derivations, it is useful to distinguish between tensile modulus E_f^t and bending modulus E_f^b of the fibre. While for the homogeneous and isotropic fibre $E_f^t = E_f^b$, this equality does not hold under sandwich beam assumption (see Section 4). The linear elastic description restricts the quantitative validity of the results to sufficiently small critical strains, although the qualitative conclusions are not expected to depend on this assumption.

3. Theoretical

The classical estimation of the buckling strain in both macroscopic and microscopic regimes for periodic layered composites was provided by Parnes and Chiskis [52], who treated the stiff layers as Euler–Bernoulli beams on an elastic foundation formed by the matrix, with the interfacial stresses obtained from an explicit plane-strain elasticity solution. This route differs from the transfer matrix formulations employed for Bloch analyses of finitely strained layered media [31,37]. Here, we rely on the method of [52], but take into account the alternating interlayer spacing: the two matrix gaps adjacent to a given layer now have different widths, and each interface therefore contributes its own foundation term. Treating the stiff layers as Euler–Bernoulli beams embedded in an elastic foundation (matrix), the equilibrium equation for the single layer in the composites under compression force P can be written as

$$\alpha \frac{d^4V(X)}{dX^4} + h_f\sigma_f \frac{d^2V(X)}{dX^2} - \frac{h_f}{2}\frac{d(\sigma_{xy}^1 + \sigma_{xy}^2)}{dX} + (\sigma_{yy}^1 + \sigma_{yy}^2) = 0, \tag{3.1}$$

where $\alpha = E_f^b h_f^3/12$ is the flexural rigidity, σ_{xy}^i and σ_{yy}^i are the shear and compressive stresses acting on the interface between stiff layer and matrix with the superscript $i = 1,2$ for left and right interfaces, respectively (see Fig. 1). From Eq. (3.1), the critical stress can be expressed as

$$\sigma_f = -\frac{1}{dV^2(X)/dX^2}\left[\frac{\sigma_{yy}^1 + \sigma_{yy}^2}{h_f} - \frac{1}{2}\frac{d(\sigma_{xy}^1 + \sigma_{xy}^2)}{dX} + \frac{E_f^b h_f^2}{12}\frac{d^4V(X)}{dX^4}\right] \tag{3.2}$$

To find the expressions for σ_{xy}^i and σ_{yy}^i, first we solve the problem for the displacement $u^i(x,y)$ and $v^i(x,y)$ in matrix (left and right parts), which are searched in form

$$u^i(x,y) = \left[B_1^i \sinh(ky) + B_2^i \cosh(ky)\right]\sin(kx) \tag{3.3}$$

$$v^i(x,y) = \left[A_1^i \cosh(ky) + A_2^i \sinh(ky)\right]\cos(kx), \tag{3.4}$$

where $k = 2\pi/L$ is the corresponding wavenumber (Fig. 1c), A_i^j and B_j^i are the constants that can be found from the Navier–Lamé equations together with the boundary conditions, namely the continuity of the displacements with the deflection of the buckled layer at the layer–matrix interfaces, as

$$A_1^i = a\frac{(R - c_f c_m^i k^2)\sinh(kc_m^i) + kc_m^i\cosh(kc_m^i)}{kc_m^i + R\sinh(kc_m^i)\cosh(kc_m^i)} \tag{3.5}$$

$$A_2^i = \frac{c_f ka\cosh(kc_m^i) - a\sinh(kc_m^i)}{kc_m^i + R\sinh(kc_m^i)\cosh(kc_m^i)} \tag{3.6}$$

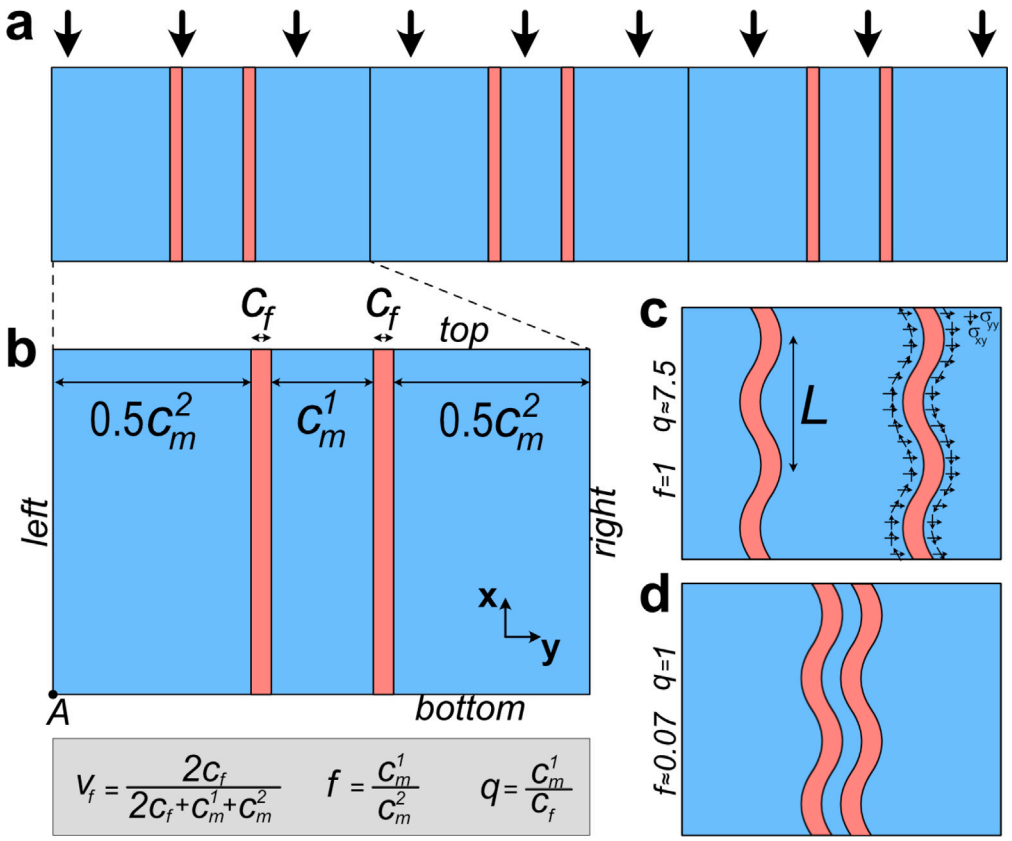


Fig. 1. (a) Schematic of the layered composite with alternating interlayer spacing and of the geometric parameters used throughout the manuscript. (b) Unit cells describing the geometry of the composite and used for Bloch–Floquet analysis. (c) The example of buckling of periodic composite ($f = 1$). (d) The example of buckling of composite with closely located layers ($q = 1$).

$$B_1^i = -\left[A_1^i + RA_2^i\right] \tag{3.7}$$

$$B_2^i = -A_2^i \tag{3.8}$$

$$R = \frac{\lambda + 3\mu}{\lambda + \mu} \tag{3.9}$$

The following expressions for stresses σ_{xy}^i and σ_{yy}^i under the assumption of linear elasticity and plane-strain conditions can be then obtained after several mathematical simplifications.

$$\sigma_{yy}^i = 2\mu k a \Theta_{yy}^i \cos(kx) \tag{3.10}$$

$$\sigma_{xy}^i = -2\mu k a \Theta_{xy}^i \sin(kx), \tag{3.11}$$

where

$$\Theta_{yy}^i = \frac{\mu\phi_f \cosh(\phi_m^i)\sinh(\phi_m^i) + (\lambda+\mu)\phi_f\phi_m^i + (\lambda+\mu)\sinh^2(\phi_m^i)}{(\lambda+3\mu)\sinh(\phi_m^i)\cosh(\phi_m^i) + \phi_m^i(\lambda+\mu)} \tag{3.12}$$

$$\Theta_{xy}^i = \frac{\phi_f(\lambda+2\mu)\cosh^2(\phi_m^i) + \mu\sinh(\phi_m^i)\cosh(\phi_m^i) + \phi_m^i(\lambda+\mu)}{(\lambda+3\mu)\sinh(\phi_m^i)\cosh(\phi_m^i) + \phi_m^i(\lambda+\mu)} \tag{3.13}$$

and $\phi_f = kc_f$, $\phi_m^i = kc_m^i$.

Applying Eq. (3.11) into Eq. (3.2) yields

$$\sigma_f = \mu\left[\Theta_{xy}^1 + \frac{1}{\phi_f}\Theta_{yy}^1\right] + \mu\left[\Theta_{xy}^2 + \frac{1}{\phi_f}\Theta_{yy}^2\right] + \frac{E_f^b\phi_f^2}{3} \tag{3.14}$$

After another series of simplifications, the final expression for the σ_f takes form

$$\sigma_f = \mu Q^1 + \mu Q^2 + \frac{E_f^b\phi_f^2}{3}, \tag{3.15}$$

where

$$Q^i = 2 + \frac{1+f_1}{\phi_f}\Psi^i \tag{3.16}$$

$$\Psi^i = \frac{(\sinh(\phi_m^i) - \phi_f\cosh(\phi_m^i))^2}{(2+f_1)\sinh(\phi_m^i)\cosh(\phi_m^i) + f_1\phi_m^i} \tag{3.17}$$

$$f_1 = \frac{\lambda+\mu}{\mu} \tag{3.18}$$

Applying Hooke's law, one can find the critical strain as

$$\varepsilon_{cr} = \Gamma\left[2 + \frac{1+f_1}{\phi_f}\left(\frac{\Psi^1+\Psi^2}{2}\right)\right] + \frac{E_f^b}{E_f^t}\frac{\phi_f^2}{3}, \tag{3.19}$$

where $\Gamma = 2\mu/E_f^t$ for plane stress and $\Gamma = 2\mu(1-\nu_f)/E_f^t$ for plane strain conditions. One may notice that Eq. (3.19) is equivalent to (2.11a) from Parnes and Chiskis [52] when $\Psi^1 = \Psi^2$, which corresponds to ideally periodic composites ($c_m^1 = c_m^2$ and $E_f^t = E_f^b$). While a rigorous term-by-term physical interpretation of Eq. (3.19) is not straightforward, the last term, proportional to ϕ_f^2, originates from the flexural rigidity and represents the resistance of the stiff layer itself to bending.

For the selected geometric parameters of the composite and elastic constants of the constituents, Eq. (3.19) still explicitly depends on the buckling wavelength. Therefore, to find the actual buckling strain, one needs to find the minimal value of ε_{cr} with respect to L (or k). In other words, the critical strain corresponds to the case, for which

$$\frac{d\varepsilon}{dk} = 0 \tag{3.20}$$

For ideally periodic composites, solving Eq. (3.20) is equivalent to solving $\frac{d\varepsilon}{d\phi_f} = 0$, as shown in [52], which is a convenient route to the analytical expressions for k_{cr} and ε_{cr}. For $v_f \to 0$ the critical $\varepsilon_{cr} \approx \left[\frac{2(2+f_1)}{3\Gamma(1+f_1)}\right]^{-2/3}$ [52]. The same routine can be applied to the composites with alternating spacing considered here: for a given geometry (parameters c_f, c_m^1, c_m^2) the minimum of Eq. (3.19) is found using Eq. (3.20).In practice, this minimum is found by evaluating Eq. (3.19)

on a fine grid of wavenumbers and taking the smallest value. The dependence is smooth and, in the microscopic regime, has a single interior minimum (Fig. 2a), so that no more elaborate optimisation is needed. In the macroscopic regime it decreases monotonically and the minimum is attained at the lower end of the considered range (Fig. 2b). A further question can also be posed for these materials: at a fixed volume fraction, which arrangement of layers yields the least and the most stable composite?

To reformulate this question in a more rigorous sense, recall that fixing v_f still leaves the parameter f free, whereas the wavenumber k remains free and is determined separately by the minimisation in Eq. (3.20). The question of which arrangement provides the least and the most stable composite at constant v_f therefore amounts to redistributing the matrix between the two gaps. This optimisation is carried out in Section 6.2, where we show that the ideally periodic arrangement is the most stable and that the lowest critical strain is reached for $q \approx 1$.

4. Theoretical sandwich beam model

As an alternate approach, for low values of f, considered composite can be treated as conventional periodic layered composites with embedded sandwich beam, an approach used to describe the buckling of a stiff lamella sandwiched between two soft layers [60]. The effective tensile $\overline{E^t}$ and bending $\overline{E^b}$ moduli can be expressed as [60,61]

$$\overline{E^t} = \frac{2E_f(c_f) + E_m(c_m^1)}{2(c_f) + (c_m^1)} \tag{4.1}$$

$$\overline{E^b} = \frac{E_f(8(c_f)^3 + 12(c_f)^2(c_m^1) + 6(c_f)(c_m^1)^2) + E_m(c_m^1)^3}{(2(c_f) + (c_m^1))^3} \tag{4.2}$$

The additional brackets are added in Eq. (4.2) to avoid confusion between superscripts and exponents. The critical strain $\overline{\varepsilon}_{cr}$ for the composite with periodically embedded sandwich beams can then be estimated by substituting the effective moduli of Eq. (4.2) into Eq. (3.19) and setting $\Psi^1 = 0$, which gives

$$\overline{\varepsilon}_{cr} = \overline{\Gamma}\left[2 + \frac{1+f_1}{\phi_f}\left(\frac{\Psi^2}{2}\right)\right] + \frac{\overline{E_f^b}}{\overline{E_f^t}}\frac{\phi_f^2}{3}, \tag{4.3}$$

where $\overline{\Gamma} = 2\mu/\overline{E_f^t}$ for plane stress and $\overline{\Gamma} = 2\mu(1-\nu_f)/\overline{E_f^t}$ for plane strain conditions. For small v_f the outer gap c_m^2 becomes much larger than the critical wavelength, so that each pair of closely spaced layers, together with the thin gap separating them, behaves as an isolated composite beam embedded in an effectively infinite matrix. At larger volume fractions the neighbouring pairs interact through the outer gap, and the overall behaviour departs from the assumed composite-beam form.

5. Numerical analysis

In order to numerically identify the onsets of instabilities, the Bloch–Floquet approach was employed with the help of finite element analysis in COMSOL 5.4a. First, the macroscopic deformation was applied by using the periodic displacement boundary conditions on the faces of unit cell (Fig. 1b). Following a mesh sensitivity analysis, the unit cell was discretised with a mapped mesh of quadrilateral elements with quadratic serendipity shape functions, refined within the smaller matrix gap, such that a further fourfold increase in the number of elements changes the computed critical strains only marginally. Once a deformed state is obtained, Bloch–Floquet conditions are imposed on the faces of unit cell as $u(X+R) = u(X)e^{-iK\cdot R}$, where X and u denote the position vector and displacement vector, respectively; K and R denote the Bloch wave vector and spatial periodicity in the reference configuration. The corresponding eigenvalue problem (see [39]) was solved for the range of wavevectors $K = (k_{cr}, 0)$ oriented along the stiff layers, that is, along the direction of the applied compression. This orientation is dictated by the physics of the problem, since the first instability corresponds to wrinkling of the stiff layers, whose modes are periodic along the layer direction, while the long-wave limit $k \to 0$ within the same family recovers the macroscopic instability, so that both regimes are captured by a single family of wavevectors. If all the computed eigenvalues remained strictly positive for all $k > 0$, the value of ε was increased and the procedure repeated until the first non-trivial zero eigenvalue was found. The $\varepsilon_{cr} = \varepsilon$ and $k_{cr} = k$ for the first found non-trivial zero eigenvalue correspond to the critical strain and critical wavenumber, respectively. For more detailed and illustrative description of the numerical procedure for search of elastic instabilities, readers are referred to Slesarenko and Rudykh [40]. Note, that here the cases of the microscopic and macroscopic (long-wave) instabilities are distinguished based on the value of k_{cr}. Microscopic instabilities, associated with the formation of wrinkling interfaces, correspond to the critical wavelength $l_{cr} = 2\pi/k_{cr}$, while the macroscopic instabilities correspond to the specific case of $k_{cr} \to 0$ and $l_{cr} \to \infty$. Numerically, the instability is classified as macroscopic when the first non-trivial zero eigenvalue is attained at the lower end of the considered range of wavenumbers, $k_{cr} < 10^{-4}$. In the latter case, in general, the onset of macroscopic instabilities can be determined through the evaluation of the effective tensor of elastic moduli and analysis of the loss of ellipticity conditions [36,40]

6. Results and discussion

6.1. Dependence on q

For a given geometry the actual buckling strain is the minimum of $\varepsilon_{cr}(k)$ over all wavenumbers, and the location of this minimum distinguishes the two types of instability. Fig. 2 illustrates the two possible cases of the dependence of ε_{cr} on the wavelength L, computed with the full analytical model, Eq. (3.19). For the microscopic case (a), the minimum is attained at a finite wavelength comparable to the size of the microstructure, so that the critical wavenumber k_{cr} is finite. For the macroscopic case (b), $\varepsilon_{cr}(k)$ decreases monotonically as the wavelength grows, and the minimum is reached only in the long-wave limit $k_{cr} \to 0$ ($L \to \infty$), which is the signature of a macroscopic, homogenised instability: in this limit the mode no longer resolves the microstructure and effectively samples the homogenised properties of the composite, in line with the equivalence between the long-wave limit of the Bloch–Floquet analysis and the loss of ellipticity of the effective moduli [36,40].

Applying this minimisation to the alternating-spacing composite reveals a feature, already hinted at in Fig. 2: bringing the two closest stiff layers together does not stabilise the composite. This can be traced directly to Eq. (3.19). Fixing the wavenumber k and the volume fraction v_f, and denoting $g = 1/q$ and $x = \phi_m^1$, the expression (3.17) associated with the smaller gap can be written as

$$\Psi^1 = \frac{g^2x^2 - 2gx\tanh(x) + \tanh^2(x)}{(2+f_1)\tanh(x) + \frac{gf_1x}{\cosh^2(x)}} \tag{6.1}$$

It is not hard to see that $\Psi^1 \to \infty$ when $g \to \infty$ (i.e. $q \to 0$) for any value of x, while Ψ^2 remains non-negative. Therefore, for any selected k and v_f, Eq. (3.19) gives $\varepsilon_{cr}(k) \to \infty$, and even its minimum over k, see Eq. (3.20), grows without a bound as $q \to 0$. In other words, the analytical model predicts that the critical strain does not saturate as the two closest layers approach each other, but instead diverges, which is not physically admissible.

Fig. 3 shows the critical strain ε_{cr} as a function of the geometric factor q for $v_f = 0.01$ and several stiffness contrasts $E_c = E_f/E_m$, and confirms this divergence. Taking the numerical results (solid symbols) as the reference, the analytical estimate, Eq. (3.19), (solid lines) slightly overestimates the critical strain. The relative error, $|\varepsilon_{cr}^{an} - \varepsilon_{cr}^{num}|/\varepsilon_{cr}^{num}$,

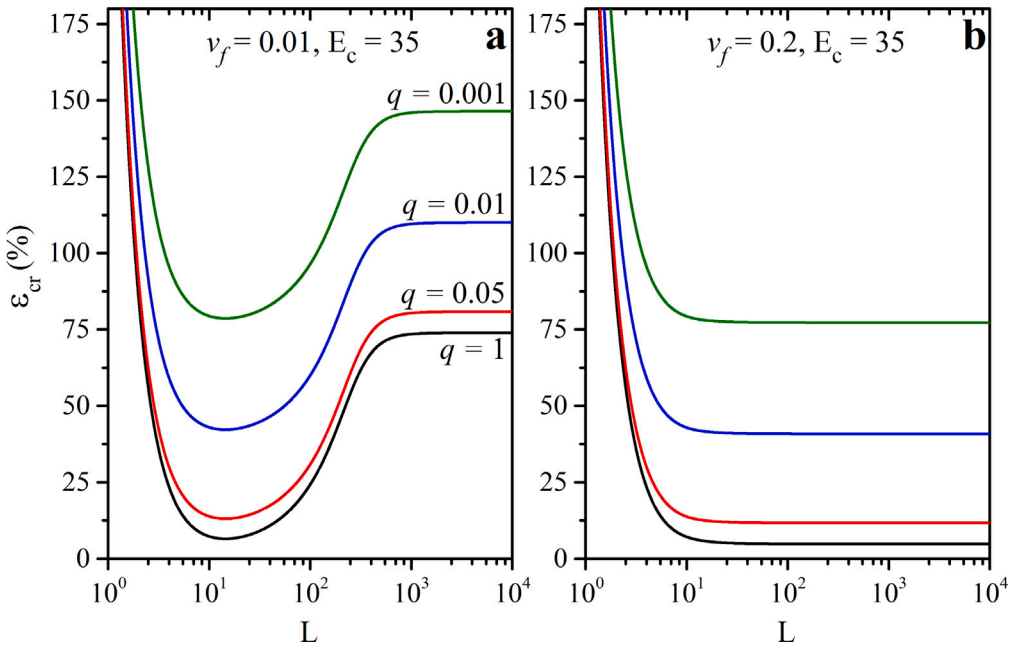


Fig. 2. Dependencies of critical strain, obtained with the full analytical model (Eq. (3.19)), on the wavelength for composites with microscopic (a) and macroscopic (b) loss of the stability.

grows with the critical strain (decreasing E_c), which stems mainly from linearisation: the equilibrium Eq. (3.1) is written in the reference configuration and the matrix response is described by small-strain elasticity, so the error grows with the magnitude of the critical strain itself. It is important to notice that the difference between the numerical (finite element) results and the theoretical models remains consistent throughout composites with various geometries (q) and elastic moduli contrasts (E_c), which allows one to draw general conclusions based on both the numerical and the theoretical results. For small enough q, however, the predicted ε_{cr} departs from the numerical values and grows without bound, which obviously cannot hold for real composites. In the extreme case when the two closest layers touch ($c_m^1 = 0$, $f = 0$), the composite recovers the classical periodicity and becomes equivalent to the periodic composite with $c_m^1 = c_m^2$ ($f = 1$) scaled by a factor of two, so that the two cases must share the same critical strain. The full model fails to reproduce this, whereas the sandwich beam model, Eq. (4.3), provides a satisfactory estimate at small q, as shown by the dashed lines. Fig. 3 thus provides a direct comparison of the two analytical descriptions against the same numerical reference: the solid curves correspond to the full model, Eq. (3.19), the dashed curves to the sandwich beam model, Eq. (4.3), and the symbols to the finite element results, for three values of the stiffness contrast.

Fig. 3 further confirms that, for the periodic case, the sandwich beam model matches the prediction of the full model (the dotted horizontal lines). The two descriptions are therefore complementary: the full model performs well for large enough distances between neighbouring layers (large q) but diverges as $q \to 0$ due to the unbounded growth of Ψ^1, while the sandwich beam model is accurate for closely located layers (small q) but not for large q, since the composite-beam kinematics underlying Eqs. (4.2) suppress the relative bending and shear of the two individual layers, so that the effective bending stiffness of the pair, and consequently the predicted critical strain, are increasingly overestimated as the inner gap widens. The value of q at which the two models are equally accurate can be obtained by equating Eqs. (3.19) and (4.3) and solving for q. Moreover, since both models overestimate the critical strain in their respective failure regimes, their lower envelope, $\bar{\varepsilon}_{cr}(q) = \min\{\varepsilon_{cr}(q), \bar{\varepsilon}_{cr}(q)\}$, provides a simple unified estimate valid over the whole range of layer arrangements, with the crossing point marking the switch between the preferred descriptions.

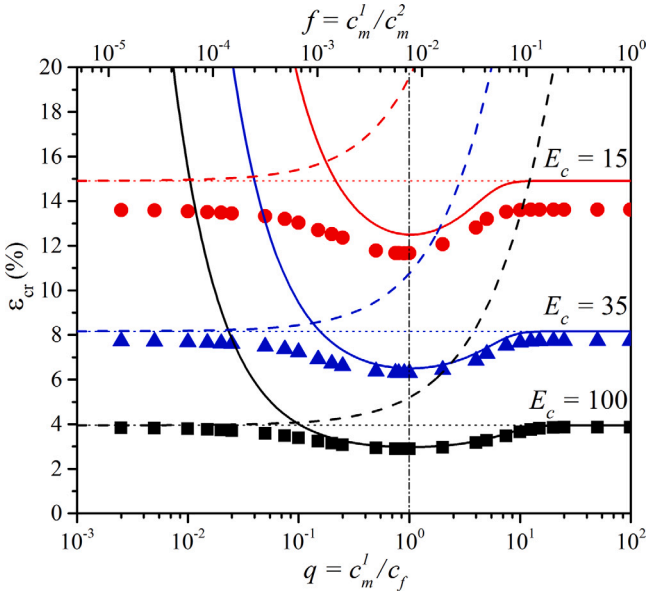


Fig. 3. Critical strain ε_{cr} vs the geometrical factor q for composites with $v_f = 0.01$ and different values of $E_c = E_f/E_m$. Symbols correspond to the numerically obtained values, solid curves represent the values obtained using Eq. (3.19), dashed curves correspond to the sandwich beam model (Eq. (4.3)), horizontal dotted curves show the value of the critical strain for ideal periodicity ($f = 1$).

6.2. Analysis of the least stable arrangement

Fig. 3 shows that the dependence of ε_{cr} on q is non-monotonic: although $\varepsilon_{cr}|_{f=0} = \varepsilon_{cr}|_{f=1}$, a minimum appears near $q \approx 1$ for all values of E_c and v_f. This can be observed both numerically and analytically from Eq. (3.19). At a fixed volume fraction and a fixed wavenumber, the only q-dependent quantity in ε_{cr} is the sum $\Psi^1 + \Psi^2$, on which ε_{cr} depends monotonically. The two gaps are not independent. With $q = c_m^1/c_f$ and $f = c_m^1/c_m^2$, the second gap follows directly as $c_m^2/c_f =$

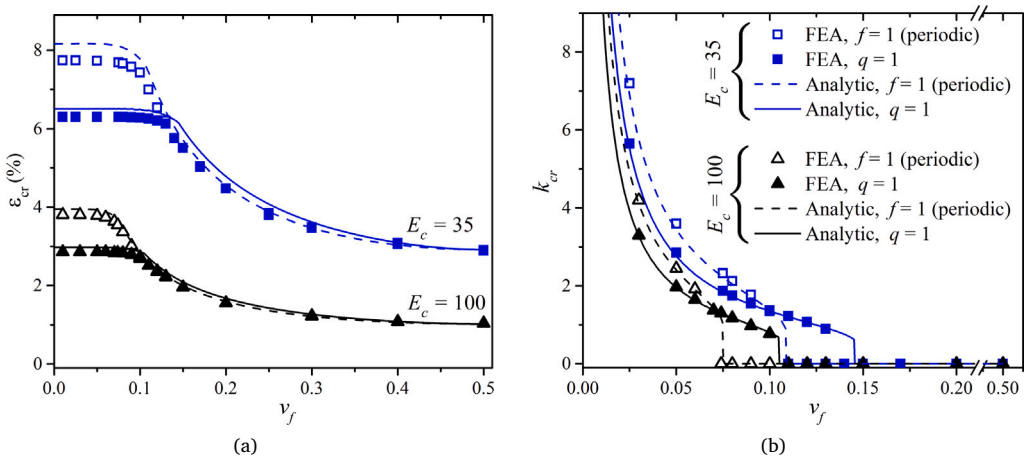


Fig. 4. Critical strain ε_{cr} (a) and critical wavenumber k_{cr} (b) as functions of the volume fraction v_f for the ideally periodic ($f = 1$; open symbols, dashed lines) and the least stable $q = 1$ (filled symbols, solid lines) arrangements. Blue squares and blue curves correspond to $E_c = 35$, black triangles and black curves to $E_c = 100$. Symbols denote the finite element results, lines the analytical predictions. The abrupt drop of k_{cr} to zero in panel (b) marks the transition from microscopic to macroscopic buckling. For both stiffness contrasts the transition occurs at a lower volume fraction for the periodic arrangement than for the $q = 1$ arrangement.

q/f, and since the volume fraction is itself a ratio of lengths, $v_f = 2c_f/(2c_f + c_m^1 + c_m^2)$, prescribing v_f and q fixes it:

$$\frac{c_m^2}{c_f} = \frac{q}{f} = \frac{2}{v_f} - 2 - q, \tag{6.2}$$

which is equivalent to the relation $f = qv_f/(2 - qv_f - 2v_f)$ introduced earlier. Identifying the least stable arrangement therefore reduces to minimising $\Psi^1 + \Psi^2$ over the admissible range $q \in (0, (1 - v_f)/v_f)$, the upper limit corresponding to the periodic case $f = 1$.

The relevant property of Ψ^i given by Eq. (3.17) is that it is non-negative and vanishes when $\tanh(\phi_m^i) = \phi_f$. For the smaller gap, $\phi_m^1 = q\,\phi_f$, this occurs at

$$q^* = \frac{\operatorname{arctanh}(\phi_f)}{\phi_f} = 1 + \frac{\phi_f^2}{3} + \dots, \tag{6.3}$$

the higher-order terms being negligible for small ϕ_f. Because the two gaps are coupled through Eq. (6.2), Ψ^1 and Ψ^2 cannot in general be minimised independently, and q^* alone need not locate the least stable arrangement. In the dilute limit, however, the second gap $c_m^2/c_f = 2/v_f - 2 - q \approx 2/v_f$ stays large and nearly constant as q is varied around unity, so that Ψ^2 remains at its wide-gap value and the minimisation of $\Psi^1 + \Psi^2$ reduces to that of Ψ^1. The least stable arrangement then coincides with q^*, which departs from unity only by $q^* - 1 \approx \phi_f^2/3$. This departure is of the order of the (small) critical strain, so the rule $q^* = 1$ becomes exact in the limit of high stiffness contrast ($\phi_f \to 0$) and accounts for the slight drift above unity seen at finite contrast in Fig. 3.

Having established that the lowest critical strain is reached for $q \approx 1$, it is valuable to follow the two limiting arrangements – the ideally periodic ($f = 1$) and the least stable ($q = 1$) – as the volume fraction of the stiff phase is varied. Fig. 4 presents the critical strain ε_{cr} (a) and the corresponding critical wavenumber k_{cr} (b) as functions of v_f for these two arrangements, for two stiffness contrasts $E_c = 35$ (blue) and $E_c = 100$ (black). The analytical predictions (lines) agree well with the finite element results (symbols).

For small volume fractions the buckling is microscopic: the critical wavenumber k_{cr} is finite, the corresponding wavelength is comparable to the size of the microstructure, and ε_{cr} is nearly independent of v_f. In this regime the $q = 1$ arrangement consistently exhibits a lower critical strain than the periodic one. As v_f increases, k_{cr} decreases and, at a certain volume fraction, reaches zero (Fig. 4b). This jump marks the transition from the microscopic (wrinkling) to the macroscopic (long-wave) instability. Beyond the transition the critical strain follows the macroscopic branch, decreases monotonically with v_f, and the difference between the two arrangements gradually vanishes.

Importantly, the transition to the macroscopic regime does not occur at the same volume fraction for the two arrangements. The periodic composite ($f = 1$) loses stability in the long-wave manner at a noticeably lower volume fraction than the $q = 1$ composite, both for $E_c = 35$ and $E_c = 100$. The macroscopic onset is controlled by the homogenised response of the composite, which at a fixed volume fraction is essentially insensitive to the arrangement of the layers, so that the long-wave branch of the critical strain is nearly identical for the two arrangements (the dashed and solid lines converge in Fig. 4a). The microscopic branch, in contrast, lies lower for the $q = 1$ arrangement, as established above. Since the transition corresponds to the crossing of the two branches, lowering the microscopic branch while leaving the long-wave branch unchanged displaces the crossing towards a higher volume fraction; the periodic composite therefore enters the macroscopic regime first. As a result, there exists a range of volume fractions in which the ideally periodic composite already buckles macroscopically, whereas the least stable $q = 1$ composite still develops a microscopic wrinkling pattern. This interplay is examined in more detail in the next subsection.

6.3. Difference between the most and the least stable states

The interplay between the arrangement of the layers and the type of the instability is summarised in Fig. 5, which maps the difference between the critical strains of the most and the least stable arrangements, $\varepsilon_{cr}^{max} - \varepsilon_{cr}^{min}$, over the volume fraction v_f and the stiffness contrast E_c. Here ε_{cr}^{max} corresponds to the ideally periodic composite ($f = 1$) and ε_{cr}^{min} to the $q = 1$ arrangement. This difference quantifies the extent to which the onset of instability can be tuned at a fixed volume fraction solely by rearranging the layers.

The difference is largest for compliant contrasts and small-to-moderate volume fractions, where it reaches up to about 4%, and it gradually decreases as either v_f or E_c increases. In the grey region the least stable ($q = 1$) arrangement itself buckles macroscopically, and the critical strain becomes essentially insensitive to q. The boundary of this region, at which the $q = 1$ composite passes from microscopic to macroscopic buckling, is indicated by the magenta dashed line.

The orange dashed line marks the analogous transition for the ideally periodic ($f = 1$) composite. As established in Section 6.2 and illustrated in Fig. 4, the periodic composite reaches the macroscopic

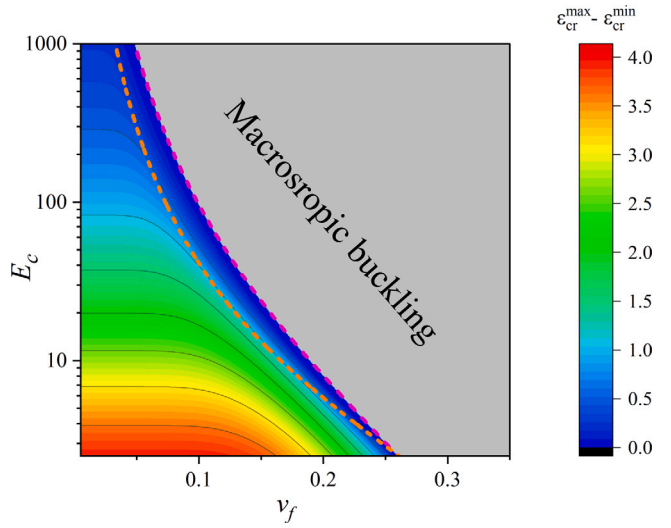


Fig. 5. Difference between the critical strains of the most ($f = 1$, ε_{cr}^{max}) and the least ($q = 1$, ε_{cr}^{min}) stable arrangements as a function of the volume fraction v_f and the stiffness contrast E_c. In the grey region the $q = 1$ arrangement buckles macroscopically and the tunability vanishes. The magenta and the orange dashed lines mark the transition from microscopic to macroscopic buckling for the $q = 1$ and for the ideally periodic ($f = 1$) arrangements, respectively. In the band between them the periodic composite is already macroscopic while the $q = 1$ composite is still microscopic.

regime at a lower volume fraction than the $q = 1$ composite, so that the orange line lies closer to the origin than the magenta one. In the band enclosed between the orange and the magenta lines the ideally periodic composite already buckles macroscopically, while the least stable $q = 1$ composite still buckles microscopically. The difference $\varepsilon_{cr}^{max} - \varepsilon_{cr}^{min}$ nevertheless remains well defined throughout this band: ε_{cr}^{max} is then the long-wave buckling strain of the periodic composite, while ε_{cr}^{min} is the microscopic wrinkling strain of the $q = 1$ composite. Only once the $q = 1$ arrangement also turns macroscopic (the grey region) does the difference becomes negligible.

The structure of this map can be related to the way the arrangement of the layers enters the critical strain, namely through the terms Ψ^1 and Ψ^2, each of which depends on the corresponding gap only through the ratio $\phi_m^i = 2\pi c_m^i / l_{cr}$ between the gap width and the buckling wavelength. The tunability appears to be largest when these two ratios are well separated, with the critical wavelength falling between the two gaps, so that the smaller gap is engaged in the interaction between the layers while the larger one is already in its saturated regime and redistributing the matrix acts on the smaller gap alone. Since $c_m^2/c_f = 2/v_f - 2 - q$, increasing the volume fraction brings the two gaps closer to each other, and the achievable difference is reduced, disappearing once the instability turns macroscopic and the critical strain is governed by the homogenised response, which at a fixed volume fraction is insensitive to the arrangement. The behaviour along the other axis has a different origin, as with increasing E_c the critical strains themselves become small, and so does the absolute difference between the two arrangements. Together, these two trends account for the shape of the tunable region in Fig. 5, which is widest at low volume fractions and compliant contrasts and narrows as either parameter increases.

Finally, since the constituents are described within linear elasticity, it is worth specifying the range in which the reported values can be treated quantitatively. For simple layered geometries the difference between the onsets predicted with Hookean and neo-Hookean phases remains minor at small and moderate deformations [40,48,51], and the present predictions are correspondingly reliable for the moderate and high stiffness contrasts, for which the critical strains stay small. For the lowest contrasts considered here the critical strains are noticeably larger, and the reported values should be regarded as linearised estimates. The qualitative conclusions — the ranking of the arrangements, the location of the least stable geometry, and the existence of a window in which the two arrangements lose stability in different ways — do not rely on the precise magnitude of the critical strain, and are therefore hold for neo-Hookean constituents as well. This extrapolation should not be extended to materials exhibiting pronounced strain stiffening, such as those described by the Gent model, since the stiffening of the phases prior to the onset alters the balance between the constituents and can shift the instability in a way that is not captured by the present analysis [42].

7. Conclusions

In this work, the elastic instabilities of layered composites with alternating interlayer spacing, in which the stiff layers are separated by two alternating gaps while the overall volume fraction is kept constant, were studied. By extending the analytical treatment of Parnes and Chiskis to this geometry, a closed-form estimate of the critical strain was derived (Eq. (3.19)) and complemented, for closely spaced layers, by a sandwich-beam model (Eq. (4.3)). The two models accurately reproduce the finite element results in their respective ranges of applicability, and together they cover the whole range of layer arrangements.

It was shown that, at a fixed volume fraction, the stability of the composite can be tuned simply by changing the relative spacing of the layers. The ideally periodic arrangement ($f = 1$) is the most stable, whereas the lowest critical strain is attained when the smallest gap becomes comparable to the layer thickness, that is for $q \approx 1$. The full analytical model captures this behaviour in the general case, and its prediction becomes more accurate the more dilute the composite and the higher the stiffness contrast.

Finally, the difference between the most and the least stable arrangements was mapped over the volume fraction–contrast plane, together with the accompanying transition between microscopic and macroscopic buckling. The two limiting arrangements do not become macroscopic simultaneously: the periodic composite enters the long-wave regime at a lower volume fraction than the $q = 1$ composite, which leaves a finite band in which the periodic composite is already macroscopically unstable while the least stable composite still wrinkles. These results demonstrate that deviations from ideal periodicity provide an additional, volume-fraction-preserving degree of freedom for controlling the onset of elastic instabilities in layered composites. From a practical point of view, if buckling is regarded as an undesired failure mode that limits the load-bearing capacity, then a critical strain computed for a perfectly periodic composite cannot be assumed to hold once the periodicity is broken: closely located layers arising during fabrication may significantly undermine the performance of the composite. It should be noted, however, that the experimental verification of this phenomenon is likely to be challenging, since the intermediate transitional layers between fibre and matrix also affect the buckling behaviour, as shown in [55].

Declaration of competing interest

The authors declare that they have no known competing financial interests or personal relationships that could have appeared to influence the work reported in this paper.

Acknowledgements

Funded by the Deutsche Forschungsgemeinschaft (DFG, German Research Foundation) under Germany's Excellence Strategy - EXC-2193/1 - 390951807. The author would like to thank the state of Baden-Württemberg for its support of bwHPC and the German Research Foundation (DFG) for funding under "Project number 455622343" (bwForCluster NEMO 2). Open access funding enabled and organised by Projekt DEAL.

Data availability

Data will be made available on request.

References

[1] R. Hill, J.W. Hutchinson, Bifurcation phenomena in the plane tension test, J. Mech. Phys. Solids 23 (4–5) (1975) 239–264, http://dx.doi.org/10.1016/0022-5096(75)90027-7.

[2] V.V. Bolotin, Delaminations in composite structures: its origin, buckling, growth and stability, Compos. Part B: Eng. 27 (2) (1996) 129–145.

[3] P.M. Reis, A perspective on the revival of structural (in)stability with novel opportunities for function: From buckliphobia to buckliphilia, J. Appl. Mech. 82 (11) (2015) 111001, http://dx.doi.org/10.1115/1.4031456.

[4] D.M. Kochmann, K. Bertoldi, Exploiting microstructural instabilities in solids and structures: From metamaterials to structural transitions, Appl. Mech. Rev. 69 (5) (2017) 050801, http://dx.doi.org/10.1115/1.4037966.

[5] J. Li, T. Dora, A. Goshkoderia, V. Slesarenko, S. Rudykh, Domain formations and pattern transitions via instabilities in soft heterogeneous materials, Adv. Mater. 31 (14) (2019) 1807309, http://dx.doi.org/10.1002/adma.201807309.

[6] J. Li, V. Slesarenko, S. Rudykh, Emergence of instability-driven domains in soft stratified materials, npj Comput. Mater. 8 (2022) http://dx.doi.org/10.1038/s41524-022-00783-x.

[7] X. Fang, D. Yu, J. Wen, Y. Dai, M.R. Begley, H. Gao, P. Gumbsch, Large recoverable elastic energy in chiral metamaterials via twist buckling, Nature 639 (8055) (2025) 639–645, http://dx.doi.org/10.1038/s41586-025-08658-z.

[8] J. Dai, L. Lu, S. Leanza, J.W. Hutchinson, R.R. Zhao, Continuous modeling of creased annuli with tunable bistable and looping behaviors, Appl. Mech. Rev. 78 (3) (2026) 030801, http://dx.doi.org/10.1115/1.4069259.

[9] K. Bertoldi, V. Vitelli, J. Christensen, M. van Hecke, Flexible mechanical metamaterials, Nat. Rev. Mater. 2 (2017) 17066, http://dx.doi.org/10.1038/natrevmats.2017.66.

[10] R. Lakes, Foam structures with a negative Poisson's ratio, Science 235 (4792) (1987) 1038–1040, http://dx.doi.org/10.1126/science.235.4792.1038.

[11] T. Mullin, S. Deschanel, K. Bertoldi, M.C. Boyce, Pattern transformation triggered by deformation, Phys. Rev. Lett. 99 (8) (2007) 084301, http://dx.doi.org/10.1103/PhysRevLett.99.084301.

[12] K. Bertoldi, P.M. Reis, S. Willshaw, T. Mullin, Negative Poisson's ratio behavior induced by an elastic instability, Adv. Mater. 22 (3) (2010) 361–366, http://dx.doi.org/10.1002/adma.200901956.

[13] B. Florijn, C. Coulais, M. van Hecke, Programmable mechanical metamaterials, Phys. Rev. Lett. 113 (17) (2014) 175503, http://dx.doi.org/10.1103/PhysRevLett.113.175503.

[14] C. Coulais, E. Teomy, K. de Reus, Y. Shokef, M. van Hecke, Combinatorial design of textured mechanical metamaterials, Nature 535 (7613) (2016) 529–532, http://dx.doi.org/10.1038/nature18960.

[15] Y. Wang, L. Li, D. Hofmann, J.E. Andrade, C. Daraio, Structured fabrics with tunable mechanical properties, Nature 596 (7871) (2021) 238–243, http://dx.doi.org/10.1038/s41586-021-03698-7.

[16] A. Farzaneh, N. Pawar, C.M. Portela, J.B. Hopkins, Sequential metamaterials with alternating Poisson's ratios, Nat. Commun. 13 (2022) 1041, http://dx.doi.org/10.1038/s41467-022-28696-9.

[17] D. Schwarz, G. Felsch, F. Tauber, S. Schiller, V. Slesarenko, Exploiting self-contact in mechanical metamaterials for new discrete functionalities, Mater. Des. 233 (2023) 112468, http://dx.doi.org/10.1016/j.matdes.2023.112468.

[18] D. Schwarz, J. Liotier, V. Slesarenko, J. Rühe, Light induced training of 3D printed mechanical metamaterials, Adv. Mater. Technol. 10 (23) (2025) 2501416, http://dx.doi.org/10.1002/admt.202501416.

[19] X. Fang, J. Wen, L. Cheng, D. Yu, H. Zhang, P. Gumbsch, Programmable gear-based mechanical metamaterials, Nat. Mater. 21 (8) (2022) 869–876, http://dx.doi.org/10.1038/s41563-022-01269-3.

[20] G. Felsch, V. Slesarenko, Generative models struggle with kirigami metamaterials, Sci. Rep. 14 (2024) 19397, http://dx.doi.org/10.1038/s41598-024-70364-z.

[21] M. Zhang, H. Shahsavan, Y. Guo, A. Pena-Francesch, Y. Zhang, M. Sitti, Liquid-crystal-elastomer-actuated reconfigurable microscale kirigami metastructures, Adv. Mater. 33 (25) (2021) 2008605, http://dx.doi.org/10.1002/adma.202008605.

[22] S. Babaee, J. Shim, J.C. Weaver, E.R. Chen, N. Patel, K. Bertoldi, 3D soft metamaterials with negative Poisson's ratio, Adv. Mater. 25 (36) (2013) 5044–5049, http://dx.doi.org/10.1002/adma.201301986.

[23] A. Rafsanjani, K. Bertoldi, Buckling-induced kirigami, Phys. Rev. Lett. 118 (8) (2017) 084301, http://dx.doi.org/10.1103/PhysRevLett.118.084301.

[24] C. Gao, V. Slesarenko, M.C. Boyce, S. Rudykh, Y. Li, Instability-induced pattern transformation in soft metamaterial with hexagonal networks for tunable wave propagation, Sci. Rep. 8 (2018) 11834, http://dx.doi.org/10.1038/s41598-018-30214-1.

[25] S. Shan, S.H. Kang, J.R. Raney, P. Wang, L. Fang, F. Candido, J.A. Lewis, K. Bertoldi, Multistable architected materials for trapping elastic strain energy, Adv. Mater. 27 (29) (2015) 4296–4301, http://dx.doi.org/10.1002/adma.201501708.

[26] P. Wang, F. Casadei, S. Shan, J.C. Weaver, K. Bertoldi, Harnessing buckling to design tunable locally resonant acoustic metamaterials, Phys. Rev. Lett. 113 (1) (2014) 014301, http://dx.doi.org/10.1103/PhysRevLett.113.014301.

[27] K. Bertoldi, M.C. Boyce, Wave propagation and instabilities in monolithic and periodically structured elastomeric materials undergoing large deformations, Phys. Rev. B 78 (18) (2008) 184107, http://dx.doi.org/10.1103/PhysRevB.78.184107.

[28] S. Rudykh, M.C. Boyce, Transforming wave propagation in layered media via instability-induced interfacial wrinkling, Phys. Rev. Lett. 112 (3) (2014) 034301, http://dx.doi.org/10.1103/PhysRevLett.112.034301.

[29] J. Li, V. Slesarenko, S. Rudykh, Auxetic multiphase soft composite material design through instabilities with application for acoustic metamaterials, Soft Matter 14 (30) (2018) 6171–6180, http://dx.doi.org/10.1039/C8SM00874D.

[30] B.W. Rosen, Mechanics of composite strengthening, in: Fiber Composite Materials, American Society for Metals, Metals Park, OH, 1965, pp. 37–75.

[31] N. Triantafyllidis, B.N. Maker, On the comparison between microscopic and macroscopic instability mechanisms in a class of fiber-reinforced composites, J. Appl. Mech. 52 (4) (1985) 794–800, http://dx.doi.org/10.1115/1.3169148.

[32] G.Y. Qiu, T.J. Pence, Loss of ellipticity in plane deformation of a simple directionally reinforced incompressible nonlinearly elastic solid, J. Elasticity 49 (1) (1997) 31–63, http://dx.doi.org/10.1023/A:1007468328031.

[33] J. Merodio, T.J. Pence, Kink surfaces in a directionally reinforced neo-hookean material under plane deformation: II. kink band stability and maximally dissipative band broadening, J. Elast. 62 (2) (2001) 145–170, http://dx.doi.org/10.1023/A:1011693326593.

[34] J. Merodio, R.W. Ogden, Material instabilities in fiber-reinforced nonlinearly elastic solids under plane deformation, Arch. Mech. 54 (5–6) (2002) 525–552.

[35] S. Rudykh, G. deBotton, Instabilities of hyperelastic fiber composites: Micromechanical versus numerical analyses, J. Elasticity 106 (2) (2012) 123–147, http://dx.doi.org/10.1007/s10659-011-9313-x.

[36] G. Geymonat, S. Müller, N. Triantafyllidis, Homogenization of nonlinearly elastic materials, microscopic bifurcation and macroscopic loss of rank-one convexity, Arch. Ration. Mech. Anal. 122 (3) (1993) 231–290, http://dx.doi.org/10.1007/BF00380256.

[37] M.D. Nestorović, N. Triantafyllidis, Onset of failure in finitely strained layered composites subjected to combined normal and shear loading, J. Mech. Phys. Solids 52 (4) (2004) 941–974, http://dx.doi.org/10.1016/j.jmps.2003.06.001.

[38] N. Triantafyllidis, M.D. Nestorović, M.W. Schraad, Failure surfaces for finitely strained two-phase periodic solids under general in-plane loading, J. Appl. Mech. 73 (3) (2006) 505–515, http://dx.doi.org/10.1115/1.2126695.

[39] K. Bertoldi, M.C. Boyce, S. Deschanel, S.M. Prange, T. Mullin, Mechanics of deformation-triggered pattern transformations and superelastic behavior in periodic elastomeric structures, J. Mech. Phys. Solids 56 (8) (2008) 2642–2668, http://dx.doi.org/10.1016/j.jmps.2008.03.006.

[40] V. Slesarenko, S. Rudykh, Microscopic and macroscopic instabilities in hyperelastic fiber composites, J. Mech. Phys. Solids 99 (2017) 471–482, http://dx.doi.org/10.1016/j.jmps.2016.11.002.

[41] J. Li, V. Slesarenko, P.I. Galich, S. Rudykh, Instabilities and pattern formations in 3d-printed deformable fiber composites, Compos. Part B: Eng. 148 (2018) 114–122, http://dx.doi.org/10.1016/j.compositesb.2018.04.049.

[42] N. Arora, J. Li, V. Slesarenko, S. Rudykh, Microscopic and long-wave instabilities in 3d fiber composites with non-gaussian hyperelastic phases, Internat. J. Engrg. Sci. 157 (2020) 103408, http://dx.doi.org/10.1016/j.ijengsci.2020.103408.

[43] J. Furer, P. Ponte Castañeda, Macroscopic instabilities and domain formation in neo-Hookean laminates, J. Mech. Phys. Solids 118 (2018) 98–114, http://dx.doi.org/10.1016/j.jmps.2018.05.006.

[44] H. Chai, D. Moshkovitz, On the post-buckling behavior of laterally constrained multilayers, Int. J. Solids Struct. 257 (2022) 111827, http://dx.doi.org/10.1016/j.ijsolstr.2022.111827.

[45] N. Arora, J. Li, S. Rudykh, Tunable buckling configurations via in-plane periodicity in soft 3D-fiber composites: Simulations and experiments, Int. J. Solids Struct. 250 (2022) 111711, http://dx.doi.org/10.1016/j.ijsolstr.2022.111711.

[46] X. Yuan, J. Huang, P. Zhao, Y. Wang, Q. Fan, Revisiting the compressive buckling of periodic multi-layers reinforced composites: Theoretical and numerical analysis, Thin-Walled Struct. 215 (2025) 113550, http://dx.doi.org/10.1016/j.tws.2025.113550.

[47] Y. Xiang, D. Chen, N. Arora, Q. Yao, S. Rudykh, Towards understanding the role of viscoelasticity in microstructural buckling in soft particulate composites, Compos. Part B: Eng. 263 (2023) 110850, http://dx.doi.org/10.1016/j.compositesb.2023.110850.

[48] V. Slesarenko, S. Rudykh, Harnessing viscoelasticity and instabilities for tuning wavy patterns in soft layered composites, Soft Matter 12 (16) (2016) 3677–3682, http://dx.doi.org/10.1039/C5SM02949J.

[49] T. Lapina, Y. Xiang, Q. Yao, D. Chen, J. Li, P. Steinmann, S. Rudykh, Microstructural buckling in soft visco-hyperelastic laminates, Int. J. Solids Struct. 311 (2025) 113242, http://dx.doi.org/10.1016/j.ijsolstr.2025.113242.

[50] V. Slesarenko, P.I. Galich, J. Li, N.X. Fang, S. Rudykh, Foreshadowing elastic instabilities by negative group velocity in soft composites, Appl. Phys. Lett. 113 (3) (2018) 031901, http://dx.doi.org/10.1063/1.5042077.

[51] J. Li, V. Slesarenko, S. Rudykh, Microscopic instabilities and elastic wave propagation in finitely deformed laminates with compressible hyperelastic phases, Eur. J. Mech. A Solids 73 (2019) 126–136, http://dx.doi.org/10.1016/j.euromechsol.2018.07.004.

[52] R. Parnes, A. Chiskis, Buckling of nano-fibre reinforced composites: A re-examination of elastic buckling, J. Mech. Phys. Solids 50 (4) (2002) 855–879, http://dx.doi.org/10.1016/S0022-5096(01)00101-6.

[53] P.I. Galich, V. Slesarenko, J. Li, S. Rudykh, Elastic instabilities and shear waves in hyperelastic composites with various periodic fiber arrangements, Internat. J. Engrg. Sci. 130 (2018) 51–61, http://dx.doi.org/10.1016/j.ijengsci.2018.05.003.

[54] A. Goshkoderia, N. Arora, V. Slesarenko, J. Li, V. Chen, A. Juhl, P. Buskohl, S. Rudykh, Tunable permittivity in dielectric elastomer composites under finite strains: Periodicity, randomness, and instabilities, Int. J. Mech. Sci. (2020) 105880, http://dx.doi.org/10.1016/j.ijmecsci.2020.105880.

[55] N. Arora, A. Batan, J. Li, V. Slesarenko, S. Rudykh, On the influence of inhomogeneous interphase layers on instabilities in hyperelastic composites, Materials 12 (5) (2019) 763, http://dx.doi.org/10.3390/ma12050763.

[56] C. Gao, Y. Li, Tuning the wrinkling patterns of an interfacial/coating layer via a regulation interphase, J. Solids Struct. 104–105 (2017) 92–102, http://dx.doi.org/10.1016/j.ijsolstr.2016.11.003.

[57] A.D. Bakiler, A. Javili, Wrinkling of a compressible trilayer domain under large plane deformations, Int. J. Solids Struct. 241 (2022) 111465, http://dx.doi.org/10.1016/j.ijsolstr.2022.111465.

[58] B. Wang, B. Zhang, H. Bi, H. Ouyang, Y. Huang, S. Wang, Theoretical predictions and evolutions of wrinkles in the film-intermediate layer-substrate structure under compression, Int. J. Solids Struct. 250 (2022) 111699, http://dx.doi.org/10.1016/j.ijsolstr.2022.111699.

[59] X. Yuan, Q. Fan, Interphase-mediated buckling behavior of soft layered composites: Theoretical modelling and simulations, Int. J. Solids Struct. 333 (2026) 113973, http://dx.doi.org/10.1016/j.ijsolstr.2026.113973.

[60] W.-H. Xie, X. Huang, Y.-P. Cao, B. Li, X.-Q. Feng, Buckling and postbuckling of stiff lamellae in a compliant matrix, Compos. Sci. Technol. 99 (2014) 89–95, http://dx.doi.org/10.1016/j.compscitech.2014.05.015.

[61] Y. Li, N. Kaynia, S. Rudykh, M.C. Boyce, Wrinkling of interfacial layers in stratified composites, Adv. Eng. Mater. 15 (10) (2013) 921–926, http://dx.doi.org/10.1002/adem.201200387.